Journal of Solid State Chemistry **148,** 63–74 (1999)
Article ID jssc.1999.8350, available online at http://www.idealibrary.com on IDEAL®

Structural and Diffraction Properties of Incommensurate Solid Inclusion Compounds Formed between α,ω-Dihalogenoalkanes and Tri-*ortho*-thymotide[1]

Heliodoro Serrano-González and Kenneth D. M. Harris[2]

School of Chemistry, University of Birmingham, Edgbaston, Birmingham B15 2TT, United Kingdom

Received January 8, 1999; accepted April 22, 1999

Structural properties of incommensurate solid inclusion compounds formed between long-chain α,ω-dihalogenoalkanes [1,10-dibromodecane, $Br(CH_2)_{10}Br$; 1,8-diiodooctane, $I(CH_2)_8I$; 1,10-diiododecane, $I(CH_2)_{10}I$] and tri-*ortho*-thymotide (TOT) are reported, together with a detailed discussion of the diffraction properties of these inclusion compounds. At ambient temperature, all three inclusion compounds have essentially the same TOT "host" structure, within which there are linear, parallel tunnels. The α,ω-dihalogenoalkane "guest" molecules form an ordered arrangement along these tunnels, with an incommensurate relationship between the periodicities of the host and guest structures along the tunnel direction. However, the guest molecules do not exhibit strong inter-tunnel ordering (in contrast to the situation for the same guest molecules in urea inclusion compounds). As a consequence of the partially disordered guest substructures in these TOT inclusion compounds, the single-crystal X-ray diffraction patterns contain substantial diffuse scattering. The results reported here provide evidence for a weak superstructure of the host in the 1,10-dibromodecane/TOT and 1,10-diiododecane/TOT inclusion compounds and evidence for a low-temperature phase transition in the 1,8-diiodooctane/TOT inclusion compound. The diffraction properties of these inclusion compounds and their corresponding structural implications are assessed in detail.

INTRODUCTION

In solid inclusion compounds of tri-*ortho*-thymotide (TOT), appropriate "guest" molecules are located within cavities or tunnels generated from the crystal packing of TOT molecules (the "host" structure). The TOT molecule (Fig. 1) is flexible, and in solution two different chiral conformations predominate (1). The major conformer is described as a "propeller," with all three carbonyl oxygen atoms pointing to one side of the central 12-membered ring. The minor conformer is described as "helical," with one carbonyl oxygen atom pointing in the opposite direction to the other two. The pure crystalline phase of TOT (2) is a racemic mixture of the two enantiomers of the propeller conformation. When TOT is crystallized in the presence of appropriate guest molecules, inclusion compounds of TOT can be formed. A wide variety of guest molecules can form such inclusion compounds with TOT, and the TOT host structure can differ substantially depending on the structural characteristics of the guest. Comprehensive reviews of solid inclusion compounds of TOT are given in Refs. (3, 4).

In general, TOT inclusion compounds can be classified as either cage type or tunnel type depending on the nature of the inclusion cavities within the host structure. In the cage-type inclusion compounds, the guest molecules are enclosed in discrete cavities within the host crystal, and guest molecules in different cages are not in direct contact with each other. Virtually all cage-type TOT inclusion compounds have space group $P3_121$, and are formed by guest molecules with maximum dimension shorter than ca. 9 Å, such as acetone, methanol, bromocyclohexane, and pyridine. In general, the cage-type inclusion compounds have a host/guest molecular ratio of 2.

The tunnel-type inclusion compounds can be subdivided into two general types, characterized by different tunnel topologies:

i. *Systems of intersecting tunnels* (denoted here as type T-I): This type of tunnel structure is typically formed with nonlinear guests such as benzene, toluene, *trans*-stilbene, and *cis*-stilbene. The space group is $P\bar{1}$ and there are three different types of tunnels in the host structure. Two types of tunnels are parallel to each other and have uniform cross-sectional areas. The third type of tunnel lies along another direction and its cross-sectional area varies, through a series of constrictions and bulges, on moving along the tunnel.

ii. *Parallel, nonintersecting tunnels* (denoted here as type T-II): This type of tunnel structure is typically formed with

[1] Dedicated to Professor C. N. R. Rao, FRS, on the occasion of his 65th birthday.

[2] To whom correspondence should be addressed: Fax: +44–121–414–7473. E-mail: K.D.M.Harris@bham.ac.uk.

0022-4596/99 $30.00

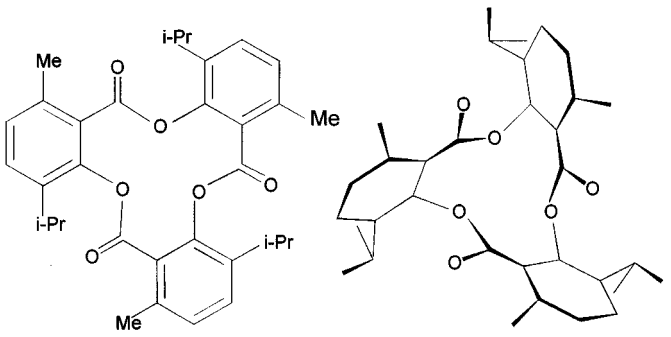

FIG. 1. Molecular structure of TOT.

long-chain, unbranched guest molecules longer than ca. 9.5 Å. Linear, parallel tunnels run through the crystal, generally along the principal crystallographic axis. The space group is usually $P6_1$ ($P6_5$), $P6_2$ ($P6_4$) or $P3_1$ ($P3_2$) depending on the guest, with the screw axis lying along the tunnel direction. The first studies of TOT inclusion compounds of type T-II, carried out by Lawton and Powell (5), investigated a range of different types of guest molecules, and the lattice parameters and space groups were characterized from single-crystal X-ray diffraction photographs. Among these guests, α,ω-dibromoalkanes [$Br(CH_2)_nBr$] with $n = 1$, 2, and 3 and α,ω-diiodoalkanes [$I(CH_2)_nI$] with $n = 1$ and 6 were studied. We note that, in common with many other solid organic inclusion compounds, the tunnels are stable only if guest molecules are present. If the guest molecules are removed (for example, by heating), the empty tunnels collapse to give the pure crystalline phase of TOT.

It is important to note that the host structure in many TOT inclusion compounds is chiral, and may influence significantly the properties of the guest molecules. For chiral guest species, one enantiomer would be expected to predominate within a given single crystal of the inclusion compound, and the opportunity for exploiting this host–guest chiral recognition has received considerable attention for TOT inclusion compounds (3, 4, 6, 7).

The work presented here is part of a comprehensive study of the structural properties of organic inclusion compounds containing tunnel host structures. Much research has been devoted to other families of solid organic inclusion compounds, particularly the urea and thiourea inclusion compounds (8), with some focus on families of inclusion compounds containing long-chain α,ω-dihalogenoalkane guest molecules. The present paper extends previous research on TOT inclusion compounds by considering TOT inclusion compounds containing long-chain α,ω-dihalogenoalkane guest molecules, with the expectation that these guest molecules will generate one-dimensional tunnel structures of type T-II, analogous to the tunnel topologies of the urea inclusion compounds. Among other aspects, the fact that the distance between adjacent tunnels in the TOT inclusion compounds (ca. 14.3 Å for type T-II) is larger than that for urea inclusion compounds (ca. 8.2 Å) may provide a systematic means of investigating the factors that influence the intertunnel ordering of the guest molecules. Concepts developed to understand the structural properties of urea inclusion compounds may be applied to other inclusion compounds with one-dimensional tunnel structures, such as the TOT inclusion compounds of type T-II. These concepts are discussed in detail in Ref. (9) and are summarized in Section 2.

In this paper, we focus on TOT inclusion compounds containing the following α,ω-dihalogenoalkane guest molecules: 1,10-dibromodecane [$Br(CH_2)_{10}Br$, abbreviated $C_{10}Br_2$], 1,8-diiodooctane [$I(CH_2)_8I$, abbreviated C_8I_2], and 1,10-diiododecane [$I(CH_2)_{10}I$, abbreviated $C_{10}I_2$]. We find that these inclusion compounds have certain structural features in common (as well as certain subtle differences) and it is convenient to discuss them together. The structural properties of other TOT inclusion compounds containing long-chain α,ω-dihalogenoalkane guest molecules (such as 1,8-dibromooctane and 1,12-dibromododecane) contrast markedly with those reported here, and will be discussed in detail elsewhere (10).

2. OVERVIEW OF STRUCTURAL ASPECTS OF TUNNEL INCLUSION COMPOUNDS

Solid inclusion compounds are composed of two chemically distinguishable subsystems: the host and guest components. For one-dimensional tunnel structures, an important classification concerns the relationship between the periodicities (denoted c_h and c_g) of the host and guest components along the tunnel axis (Fig. 2). The relationship is commensurate if sufficiently small integers (p and q) can be found such that $pc_h \approx qc_g$, and incommensurate if sufficiently small integers cannot be found to satisfy this equation. The commensurate or incommensurate nature of the inclusion compound has important implications with respect to the structural and dynamic properties of the inclusion compound. We note that other criteria, based on the energetics of host–guest interaction, have been developed (11) for distinguishing commensurate and incommensurate behavior.

With respect to structure determination, a commensurate inclusion compound can be understood as a single composite system, with periodicity described by a three-dimensional lattice and symmetry described by a three-dimensional space group. For a commensurate system, it is not necessary to delineate any explicit structural distinction between the host subsystem and the guest subsystem. In reciprocal space, all diffraction maxima can be rationalized on the basis of a conventional three-dimensionally periodic reciprocal lattice, which can be rationalized completely in terms of diffraction from the composite inclusion compound

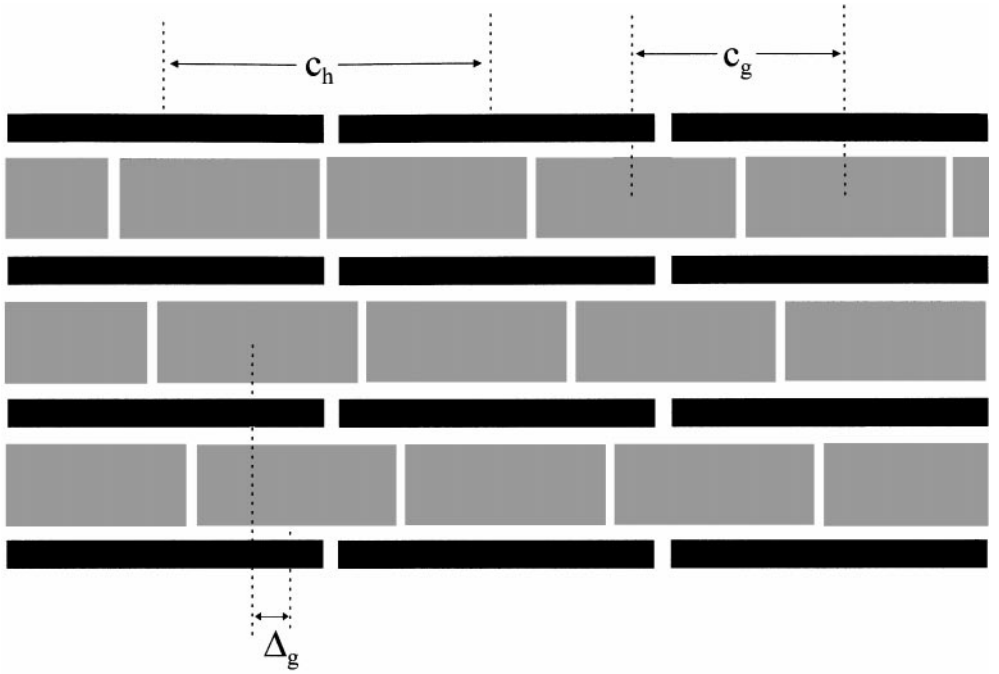

FIG. 2. Schematic two-dimensional representation of a tunnel inclusion compound, viewed perpendicular to the tunnel axis, indicating the definitions of c_g and c_h.

(with no requirement to attribute separate contributions to the diffraction pattern from the host and guest subsystems).

For an incommensurate inclusion compound, on the other hand, the composite system does not have periodicity described by a conventional three-dimensional lattice nor symmetry described by a conventional three-dimensional space group. Instead, four (or more) basis reciprocal lattice vectors are required to define the structural periodicity, and a four-dimensional (or higher-dimensional) superspace group (12) is required to describe the overall symmetry of the composite inclusion compound. As a first step toward understanding the structural properties of an incommensurate inclusion compound, it is convenient to step back from the superspace description of the composite system and to consider that the inclusion compound is composed of two separate (but not independent) substructures—the host substructure and the guest substructure—intergrown within each other. Such a description is particularly appropriate when, as in the present case, one substructure (the guest substructure) is substantially less well ordered than the other substructure.

In this description, each substructure is considered in terms of a basic structure that is subjected to an incommensurate modulation. In general, each basic structure has periodicity described by a conventional three-dimensional lattice and symmetry described by a conventional three-dimensional space group (although in practice the basic guest structure is often substantially disordered). The incommensurate modulation to a given basic structure represents the structural perturbations that it experiences due to its interaction with the other basic structure (i.e., host–guest interaction). The diffraction pattern can be described in terms of two interrelated scattering components, which we call the "h" and "g" diffraction patterns. The "h" diffraction pattern (denoted by subscript h) results from scattering by the basic host structure (and by the incommensurate modulation to the basic guest structure), whereas the "g" diffraction pattern (denoted by subscript g) results from scattering by the basic guest structure (and by the incommensurate modulation to the basic host structure).

In general, analysis of the "h" diffraction pattern (as described in Section 4.2) allows the basic host structure to be determined, but also provides some information concerning the guest substructure, as now described. First, for a structure with tunnels along the c axis, the $(hk0)$ reflections are common to the "h" and "g" diffraction patterns and provide two-dimensional information on the basic host structure and the basic guest structure projected onto the plane perpendicular to the tunnel axis. Second, the $(hkl)_h$ reflections with $l \neq 0$ convey information on the incommensurate perturbations to the basic guest structure (these perturbations, which arise from host–guest interaction, have the same periodicity as the basic host structure). This "perturbation electron density" represents the difference in electron density between the true guest substructure averaged over the periodicity of the basic host structure and the basic

guest structure averaged over the periodicity of the basic host structure. In general, the basic host structure alone usually accounts for the majority of the intensity of the reflections in the "h" diffraction pattern.

In principle, measurement and analysis of the "g" diffraction pattern should allow the basic guest structure to be determined. Unfortunately, the opportunities to determine the basic guest structures of incommensurate tunnel inclusion compounds are often limited by the fact that the number of well-defined Bragg diffraction maxima in the "g" diffraction pattern is usually very small. Nevertheless, in some cases (13–15), it may be possible to determine the periodicity of the basic guest structure and, thus, establish the mode of intertunnel ordering of the guest molecules.

To gain an overall (qualitative) impression of the structural properties of tunnel inclusion compounds, X-ray diffraction oscillation photographs recorded for a single crystal oscillating about the tunnel axis are particularly informative. Among other information, such photographs allow an assessment of the commensurate/incommensurate nature of the inclusion compound (the periodicities c_h and c_g may be determined directly from such photographs). For an incommensurate tunnel inclusion compound, the layer lines of the "h" diffraction pattern usually comprise sharp, discrete diffraction maxima, arising predominantly from the three-dimensionally ordered basic host structure. In general, the layer lines of the "g" diffraction pattern may contain both diffuse and discrete scattering, depending on the extent and nature of the ordering within the basic guest structure. Sheets of diffuse scattering perpendicular to the tunnel axis signify one-dimensional ordering of the guest molecules along the tunnel (9), whereas discrete Bragg scattering is characteristic of three-dimensional ordering of the guest molecules (i.e., intertunnel ordering in addition to ordering along the tunnel).

3. EXPERIMENTAL

TOT was synthesized from thymol following the procedure reported in Ref. (16). The α,ω-dihalogenoalkanes (1,10-dibromodecane, 1,8-diiodooctane, 1,10-diiododecane) were obtained commercially. To prepare the inclusion compounds, solutions of TOT dissolved in the guest species (as solvent) were prepared, and crystallization was allowed to occur by slow evaporation of solvent from these solutions at 55°C. The use of the α,ω-dihalogenoalkane as the solvent in this way is preferable over alternative procedures (such as using both TOT and the α,ω-dihalogenoalkane as solutes in another solvent) as it avoids competition between different potential guest molecules (the solvent and the α,ω-dihalogenoalkane) when forming the inclusion compound. After sufficiently large crystals had grown, they were collected and washed with 2,2,4-trimethylpentane. Powder X-ray diffraction data recorded at ambient temperature for these samples were consistent with the hexagonal type T-II phase of TOT inclusion compounds. There was no evidence for the pure crystalline phase of TOT.

Structural properties of the α,ω-dihalogenoalkane/TOT inclusion compounds were investigated by single-crystal X-ray diffraction (using oscillation photographs to assess the overall diffraction properties and diffractometric data collection for structure determination). Single-crystal X-ray diffraction data collections were carried out using graphite-monochromated Mo$K\alpha$ radiation on a Rigaku R-Axis II diffractometer equipped with an area detector. Data collections comprised 18 frames, each recorded over an oscillation range of 10°, with crystal-to-detector distance of 100 mm and exposure time of 20 min. Data collection parameters for $C_{10}Br_2$/TOT, C_8I_2/TOT, and $C_{10}I_2$/TOT at 293 K are summarized in Table 1. Crystal structure refinement calculations were carried out using the SHELXL-93 (17) and SHELXL-97 (18) programs.

Single-crystal X-ray diffraction oscillation photographs [with rotation axis parallel to the main axis of the hexagonal crystal morphology (tunnel axis of the TOT host structure)] were recorded on a Rigaku R-Axis II diffractometer (at 293 K and selected low temperatures) as follows: $C_{10}Br_2$/TOT [Cu$K\alpha_1$ radiation, crystal-to-detector distance 60 mm], C_8I_2/TOT [Mo$K\alpha$, 120 mm], and $C_{10}I_2$/TOT [Cu$K\alpha_1$, 60 mm]. A standard MSC low-temperature device was used for experiments below ambient temperature (the stability and accuracy of the low-temperature device have been determined to be ± 2 K). For $C_{10}I_2$/TOT, de Jong-Bouman single-crystal X-ray diffraction photographs were also recorded at 293 K on a Stoe Reciprocal Lattice Explorer using Ni-filtered Cu$K\alpha$ radiation.

Although we focus here on structural properties at ambient temperature (293 K), preliminary investigations of C_8I_2/TOT and $C_{10}I_2$/TOT below ambient temperature have been carried out. Differential scanning calorimetry (DSC) studies of C_8I_2/TOT and $C_{10}I_2$/TOT were carried out between 293 and 123 K (cooling rate, 20 K min^{-1}) on a Perkin Elmer Pyris 1 instrument. For C_8I_2/TOT, an exotherm is evident at about 136 K (peak maximum temperature). For $C_{10}I_2$/TOT, on the other hand, no exotherms or endotherms were observed in the temperature range studied.

4. RESULTS AND DISCUSSION

4.1. Qualitative Assessment of Diffraction/Structural Properties

a. $C_{10}Br_2$/TOT. The X-ray diffraction oscillation photograph (Fig. 3a) recorded at 293 K for a single crystal of $C_{10}Br_2$/TOT rotating about its tunnel axis reveals two separate diffraction patterns assigned as the "h" and "g" diffraction patterns of an incommensurate system. The "h"

TABLE 1
Data Collection and Refinement Parameters for Crystal Structure Determination of $C_{10}Br_2$/TOT, C_8I_2/TOT, and $C_{10}I_2$/TOT at 293 K

	Compound		
	$C_{10}Br_2$/TOT	C_8I_2/TOT	$C_{10}I_2$/TOT
Temperature	293(2) K	293(2) K	293(2) K
Wavelength	0.71069 Å	0.71069 Å	0.71069 Å
Space group	$P6_1$	$P6_1$	$P6_1$
Unit cell parameters	$a = 14.294(2)$ Å	$a = 14.319(1)$ Å	$a = 14.285(3)$ Å
	$c = 29.039(4)$ Å	$c = 29.111(2)$ Å	$c = 29.122(7)$ Å
Unit cell volume	5139(1) Å^3	5169.1(7) Å^3	5146(2) Å^3
θ range for data collection	1.64°–22.42°	1.64°–22.03°	1.65°–22.14°
Index ranges	$-15 \le h \le 14$	$-15 \le h \le 15$	$-15 \le h \le 14$
	$-14 \le k \le 15$	$-15 \le k \le 14$	$-14 \le k \le 14$
	$-31 \le l \le 28$	$-30 \le l \le 30$	$-31 \le l \le 28$
Reflections collected	14,168	17,425	12,482
Independent reflections	3902 ($R_{int} = 0.063$)	4026 ($R_{int} = 0.046$)	3607 ($R_{int} = 0.059$)
Refinement method	Full-matrix least squares on F^2	Full-matrix least squares on F^2	Full-matrix least squares on F^2
Data/restraints/parameters	3902/52/340	4026/52/370	3607/52/379
Goodness-of-fit on F^2	1.258	1.138	1.308
Final R indices [$I > 2\sigma(I)$]	$R = 0.130$	$R = 0.110$	$R = 0.150$
	w$R = 0.272$	w$R = 0.309$	w$R = 0.296$
R indices (all data)	$R = 0.132$	$R = 0.111$	$R = 0.152$
	w$R = 0.273$	w$R = 0.310$	w$R = 0.297$
Absolute structure parameter	3(4)	1(4)	2(5)
Largest difference map peak	0.197 e Å^{-3}	0.334 e Å^{-3}	0.247 e Å^{-3}
Largest difference map hole	-0.211 e Å^{-3}	-0.216 e Å^{-3}	-0.235 e Å^{-3}

diffraction pattern comprises discrete Bragg maxima and is consistent with the standard cell for TOT inclusion compounds of type T-II, whereas the "g" diffraction pattern comprises layers of diffuse scattering. The ratio of the periodicities of the basic host and basic guest structures along the tunnel direction is estimated to be $c_g/c_h \approx 0.54$, corresponding to an incommensurate relationship.

Within the diffuse scattering in the $(hk1)_g$ layer, broad local intensity maxima (which may represent broad Bragg maxima) can be identified. Thus, in addition to the

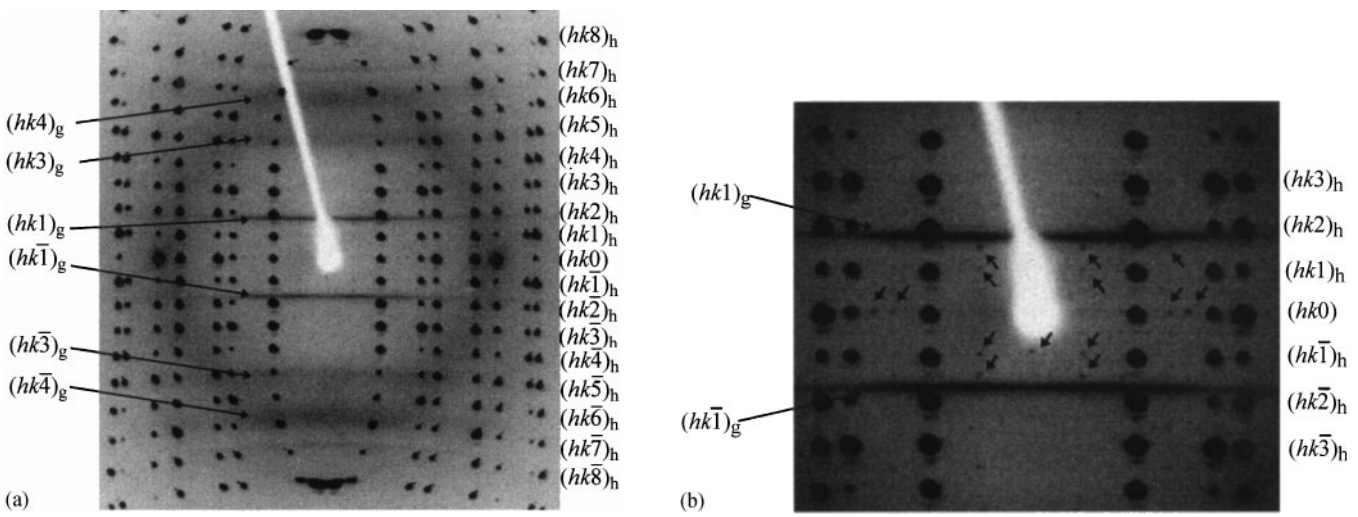

FIG. 3. (a) Oscillation photograph (with oscillation range 120°) recorded for a single crystal of $C_{10}Br_2$/TOT oscillating about its tunnel axis at 293 K. The curvature of the layer lines [except for the $(hk0)$ layer] arises from the use of a flat detector. (b) Detail of the low-angle region of a long- exposure oscillation photograph of the type shown in (a). Additional superstructure reflections are indicated by arrows.

one-dimensional ordering of the guest molecules along the tunnel direction (giving rise to the layers of diffuse scattering), there is evidence for some extent of three-dimensional ordering of the guest molecules (representing weak intertunnel ordering). In contrast, strong three-dimensional ordering of the guest molecules would give rise to sharp Bragg maxima in the "g" diffraction pattern, as observed for some urea inclusion compounds (13–15). The other layer lines with significant intensity in the "g" diffraction pattern [$(hk3)_g$ and $(hk4)_g$] represent diffuse scattering, with no local intensity maxima discernible within these layers.

On close inspection of the low-angle region of oscillation photographs recorded with long exposure time, additional very weak reflections are evident (Fig. 3b) between the layer lines of the "h" diffraction pattern and within the $(hk0)$ layer [note that these supercell reflections are very weak in comparison with other reflections in the "h" diffraction pattern]. These additional reflections are not indexed by the standard T-II cell, and are attributed to a weak supercell of the basic host structure. The supercell has been determined by comparing the 2θ values extracted from the oscillation photograph and calculated 2θ values based on plausible supercells. From this analysis, the supercell $\{\mathbf{a}, \mathbf{b}, \mathbf{c}\}$ is related in the following way to the lattice parameters $\{\mathbf{a}_s, \mathbf{b}_s, \mathbf{c}_s\}$ of the standard T-II cell,

$$\mathbf{a} = -\mathbf{a}_s - 2\mathbf{b}_s,$$

$$\mathbf{b} = 2\mathbf{a}_s + \mathbf{b}_s,$$

$$\mathbf{c} = 2\mathbf{c}_s,$$

with the following relationships between the magnitudes of the cell edges:

$$a = b = \sqrt{3}\, a_s = \sqrt{3}\, b_s,$$

$$c = 2c_s.$$

The relationship in the ab plane between the supercell and the standard T-II cell is shown in Fig. 4.

b. C_8I_2/TOT. The X-ray diffraction oscillation photograph (Fig. 5a) recorded at 293 K for a single crystal of C_8I_2/TOT oscillating about its tunnel axis is similar to that for $C_{10}Br_2$/TOT at 293 K. Two separate diffraction patterns are clearly distinguished, and are assigned as the "h" and "g" diffraction patterns of an incommensurate system. The "h" diffraction pattern comprises discrete Bragg maxima and is consistent with the standard cell for TOT inclusion compounds of type T-II, whereas the "g" diffraction pattern comprises layers of diffuse scattering. From the oscillation photograph, the following incommensurate relationship is deduced: $c_g/c_h \approx 0.53$.

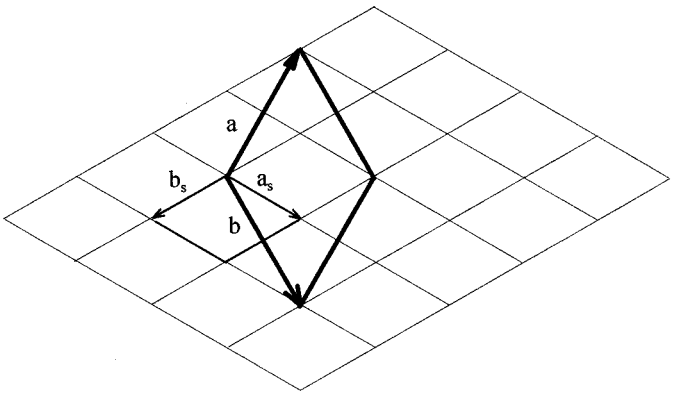

FIG. 4. Relationship between the lattice vectors $\{\mathbf{a}, \mathbf{b}\}$ of the supercell for $C_{10}Br_2$/TOT (and $C_{10}I_2$/TOT) and the lattice vectors $\{\mathbf{a}_s, \mathbf{b}_s\}$ of the standard T-II cell.

As observed for $C_{10}Br_2$/TOT, the diffuse scattering in the $(hk1)_g$ layer has fluctuations in intensity, representing broad local intensity maxima. Thus, in addition to the one-dimensional ordering of the guest molecules (giving rise to the layers of diffuse scattering) along the tunnel direction, there is evidence for some extent of three-dimensional ordering of the guest molecules (representing weak intertunnel ordering). The $(hk2)_g$ and $(hk3)_g$ layers are very weak, whereas the $(hk4)_g$ layer is stronger. No local intensity maxima are discernible in this diffuse $(hk4)_g$ layer.

The oscillation photograph recorded at 123 K (Fig. 5b) reveals changes (particularly in the high-angle region) in comparison with the oscillation photograph recorded at 293 K, indicating structural changes on lowering the temperature. This result is consistent with our DSC experiments, which provide evidence for a phase transition at about 136 K. In part, the changes observed in the diffraction pattern (Fig. 5b) on cooling may arise from twinning of the crystal on entering the low-temperature phase (as commonly observed for solid state phase transitions). Attempts to determine the lattice parameters at 123 K (and subsequently to carry out a complete data collection with a view to structure determination) were unsuccessful. In view of these problems, our future strategy to characterize the structural properties of the low-temperature phase of C_8I_2/TOT will focus on powder diffraction techniques (which are not limited by the occurrence of crystal twinning).

With respect to the "g" diffraction pattern, the oscillation photograph recorded at 123 K shows increased localization of intensity within the $(hk1)_g$ layer line, suggesting an increase in the extent of three-dimensional ordering of the guest molecules. Furthermore, additional layers of diffuse scattering are discernible at high angle [for example, on either side of the $(hk4)_g$ layer]; the positions of these additional layer lines, which are particularly broad along the

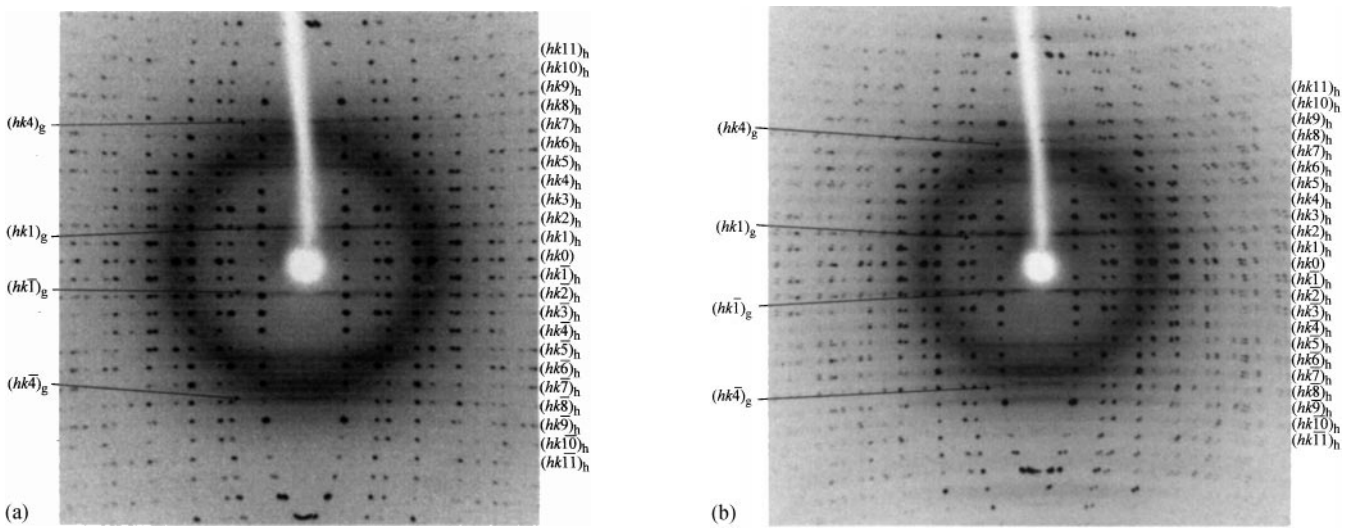

FIG. 5. Tunnel-axis oscillation photographs (with oscillation range 120°) recorded for a single crystal of C_8I_2/TOT at (a) 293 K and (b) 123 K.

$\mathbf{c}_g^*$ direction (vertical in Fig. 5b), imply a doubling of the periodic repeat distance of the guest molecules along the tunnel.

c. $C_{10}I_2$/TOT. The X-ray diffraction oscillation photograph (Fig. 6a) recorded at 293 K for a single crystal of $C_{10}I_2$/TOT oscillating about its tunnel axis is similar to those for $C_{10}Br_2$/TOT and C_8I_2/TOT at 293 K. Two separate diffraction patterns are clearly distinguished and are assigned as the "h" and "g" diffraction patterns of an incommensurate system. Again, the "h" diffraction pattern comprises discrete Bragg maxima and is consistent with the standard cell for TOT inclusion compounds of type T-II, whereas the "g" diffraction pattern comprises layers of predominantly diffuse scattering. From this oscillation photograph, the following incommensurate relationship is deduced: $c_g/c_h \approx 0.61$.

Although the $(hk1)_g$ layer line is predominantly diffuse, local intensity maxima are clearly evident, suggesting some extent of three-dimensional ordering of the guest molecules. These broad peaks appear to be more intense and localized than those in the $(hk1)_g$ layers for $C_{10}Br_2$/TOT and C_8I_2/TOT at 293 K. However, studies of the $(hk1)_g$ layer of $C_{10}I_2$/TOT using de Jong–Bouman photography at 293 K did not provide sufficient information on the distribution of the local intensity maxima to deduce the mode of intertunnel ordering of the guest molecules.

A noteworthy feature of the oscillation photograph for $C_{10}I_2$/TOT at 293 K, which we have not previously observed for one-dimensional inclusion compounds, concerns the complicated intensity distribution of the $(hk5)_g$ layer line, which may be described as two sublayers (Fig. 6a). These sublayers occur slightly above and slightly below the position predicted for the $(hk5)_g$ layer. We refer to these sublayers as $(hk5)_{g1}$ [closer to $(hk0)$] and $(hk5)_{g2}$ [further from $(hk0)$]. The origin of these two sublayers is not clear, and accurate analysis of the diffuse scattering in the $(hk5)_g$ layer (and particularly its dependence on position along the $\mathbf{c}_g^*$ direction) is required (see Section 5). Furthermore, the layer lines of the "g" diffraction pattern can be subdivided into those [$(hk3)_g$, $(hk4)_g$, and $(hk5)_{g2}$] with broad diffuse scattering along the $\mathbf{c}_g^*$ direction and those [$(hk1)_g$, $(hk5)_{g1}$] that are much sharper along the $\mathbf{c}_g^*$ direction.

As observed for $C_{10}Br_2$/TOT at 293 K, close inspection of the low-angle region of oscillation photographs recorded with long exposure time reveals reflections in between the layer lines of the "h" diffraction pattern and within the $(hk0)$ layer (Fig. 6b). These reflections arise from a weak supercell of the average basic host structure and can be indexed using the supercell described above for $C_{10}Br_2$/TOT. These additional reflections are also observed at 123 K.

At 123 K, the oscillation photograph (Fig. 6c) for $C_{10}I_2$/TOT shows increased localization of intensity in the $(hk1)_g$ and $(hk5)_{g1}$ layers, suggesting an increased extent of three-dimensional ordering of the guest molecules. Nevertheless, it is clear from the diffuse scattering that the guest substructure is still substantially disordered. As observed for the $(hk5)_g$ layer at 293 K, the $(hk3)_g$ and $(hk5)_g$ layers at 123 K can be described in terms of two closely spaced sublayers of diffuse scattering. These sublayers occur slightly above and slightly below the positions predicted for the $(hk3)_g$ and $(hk5)_g$ layers. Again, different layers in the "g"

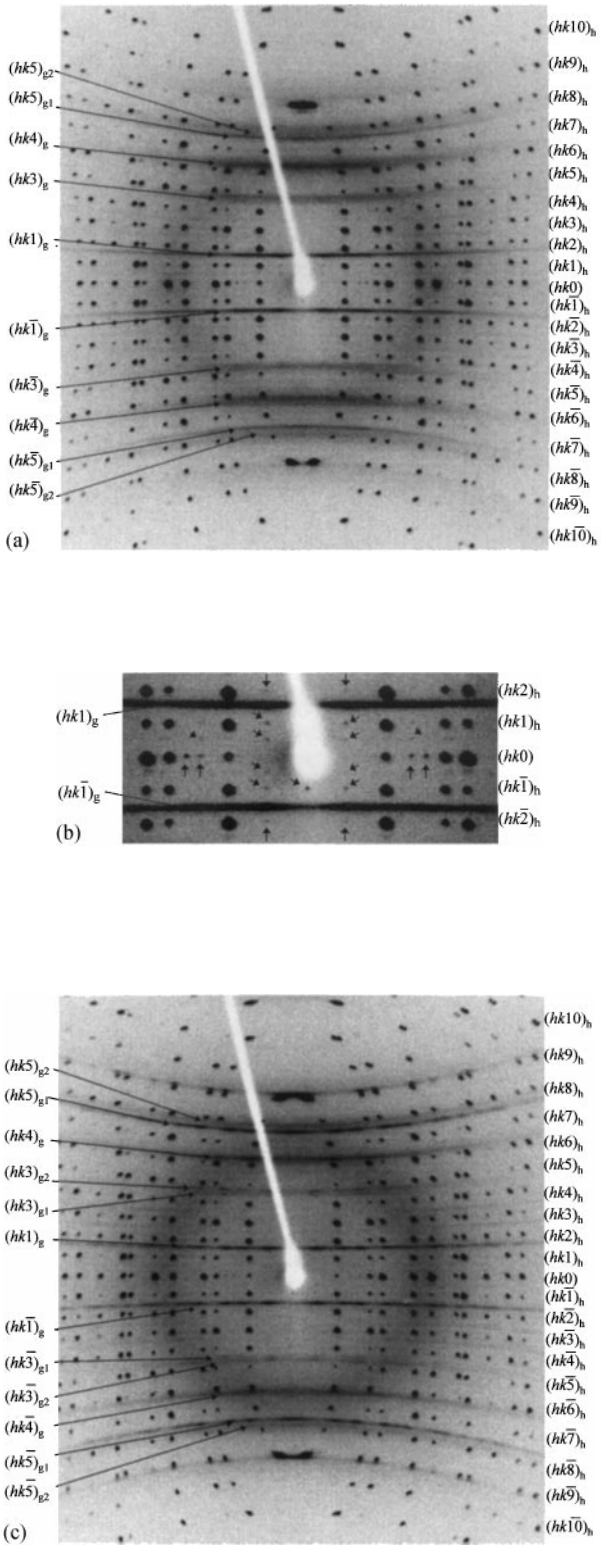

FIG. 6. Tunnel-axis oscillation photographs (with oscillation range 120°) recorded for a single crystal of $C_{10}I_2$/TOT at (a) 293 K, (b) 293 K [a long-exposure oscillation photograph, as in (a), showing detail of the low-angle region; additional superstructure reflections are indicated by arrows], and (c) 123 K.

diffraction pattern display different features. In this case, there are prominent (although broad) local intensity maxima in the $(hk1)_g$ and $(hk5)_{g1}$ layers. The sublayers $(hk3)_{g1}$ and $(hk3)_{g2}$ show similar features, but weaker than those observed for $(hk1)_g$ and $(hk5)_{g1}$. Again, the $(hk5)_{g2}$ layer is substantially broader along the $\mathbf{c}_g^*$ direction than the $(hk5)_{g1}$ layer. More detailed explorations of these regions of reciprocal space, including systematic scanning of the two-dimensional intensity distributions within these layers and sublayers, are required to establish the structural origins of these diffraction features.

4.2. Determination of the Basic Host Structures

The "h" diffraction patterns of $C_{10}Br_2$/TOT, C_8I_2/TOT, and $C_{10}I_2$/TOT at 293 K can all be indexed by a lattice with hexagonal metric symmetry ($a \approx 14.3$ Å, $c \approx 29.2$ Å; see Table 1) consistent with the standard cell (5) for TOT inclusion compounds of type T-II. In all cases, the diffraction data are consistent with Laue group $6/m$ and space group $P6_1$ (or $P6_5$). Density considerations suggest that there is one TOT molecule in the asymmetric unit. Note that for $C_{10}Br_2$/TOT and $C_{10}I_2$/TOT, the very weak superstructure reflections discussed above were not taken into account in this analysis. In part, this was because the indexing software on the diffractometer used in this study did not permit the inclusion of these very weak reflections in the indexing scheme. In any case, the number of these additional reflections is very small and their intensities are very low, and the superstructure that they allude to must therefore constitute only a minor perturbation to the basic host structure based on the standard type T-II cell. In view of the complications (see below) in structure refinements arising from the requirement to include contributions to the "h" diffraction pattern from scattering by the guest substructure, it is unlikely that the refinement calculations could sustain the introduction of additional refinable parameters to represent a weak superstructure of the basic host structure.

For $C_{10}Br_2$/TOT, attempts to solve the basic host structure by direct methods using the measured "h" diffraction data were unsuccessful. Instead, the basic host structure of the 1,8-dibromooctane/TOT inclusion compound at 293 K (10) (comprising one TOT molecule in the asymmetric unit) was used as the starting model for structure refinement of $C_{10}Br_2$/TOT. In the initial refinements, the TOT molecule was highly constrained: the benzene rings were constrained to be perfect hexagons, the atoms bonded to the benzene rings were restrained to be coplanar with the benzene ring and restrained to be positioned on the bisector of the angle formed by the relevant C–C–C unit of the benzene ring, and bond distances of the same type (for example, all C=O bonds, all C_{ring}–C_{methyl} bonds, all C–O bonds, etc.) within a TOT molecule were restrained to be equal. Ultimately,

anisotropic displacement parameters were refined for all nonhydrogen atoms. After a few cycles of refinement, the highest peaks in the difference Fourier map were located in the tunnel, representing the contribution to the "h" diffraction pattern from scattering by the guest molecules. To take account of this "perturbation guest electron density" [see Section 2 and Ref. (9)], a carbon atom was incorporated into the refinement at the position of the highest peak in the difference Fourier map, and ultimately anisotropic displacement parameters were refined. The same procedure was followed until the highest peak in the difference Fourier map was not located inside the tunnel (corresponding to a hydrogen atom of TOT). At this stage, six carbon atoms had been introduced into the tunnel to represent the contribution to the "h" diffraction pattern from scattering by guest electron density. Next, hydrogen atoms of the TOT molecule were introduced using a riding model. Attempts to relax the constraints described above resulted in some implausible bond distances and angles. The final refinement parameters are given in Table 1 and the final refined coordinates are reported in Table 2.

For C_8I_2/TOT, attempted structure solution by direct methods using the measured "h" diffraction data, and assuming a total electron density equivalent to one molecule of TOT in the asymmetric unit, was unsuccessful. However, by specifying sufficient additional electron density (representing the contribution to the "h" diffraction pattern from scattering by the guest molecules), a structure solution containing all nonhydrogen atoms of the TOT molecule was obtained. In the initial structure refinement, the geometry of the TOT molecule was subjected to appropriate constraints/restraints. Thus, the benzene rings were constrained to be perfect hexagons, the atoms attached to the benzene rings were restrained to lie in the plane of the benzene ring, the substituents of the benzene ring carbons were restrained to lie on the bisector of the angle formed by the relevant C–C–C unit of the benzene ring, and all bond distances were restrained against standard values (19). Ultimately, anisotropic displacement parameters were refined for all nonhydrogen atoms of the TOT molecules. After a few cycles of refinement, the highest peaks in the difference Fourier map were located in the tunnel, representing the contribution to the "h" diffraction pattern from scattering by the guest molecules. To take account of this "perturbation guest electron density," the procedure described above for $C_{10}Br_2$/TOT was followed until the highest peak in the difference Fourier map was not located inside the tunnel (corresponding to a hydrogen atom of TOT). At this stage, all hydrogen atoms of the TOT molecule were introduced using a riding model. The final refinement parameters are given in Table 1 and the final refined coordinates are reported in Table 3. The average basic host structure of C_8I_2/TOT is shown in Fig. 7, viewed along the *c* axis (tunnel axis).

TABLE 2
Atomic Coordinates and Equivalent Isotropic Displacement Parameters (U_{eq}) for the Average Basic Host Structure of $C_{10}Br_2$/TOT at 293 K[a]

Atom	*x*	*y*	*z*	U_{eq} (Å^2)
O(1)	0.3229(5)	0.4222(5)	0.1118(2)	0.055(2)
O(2)	0.3011(7)	0.5408(7)	0.1520(3)	0.106(3)
O(3)	0.2362(5)	0.4756(4)	0.0309(2)	0.060(2)
O(4)	0.2513(7)	0.6346(6)	0.0390(3)	0.098(3)
O(5)	0.4615(6)	0.5576(4)	0.0455(2)	0.068(2)
O(6)	0.5402(8)	0.7136(6)	0.0804(3)	0.106(3)
C(1)	0.4286(5)	0.3939(4)	0.16753(15)	0.066(3)
C(2)	0.5267(6)	0.4265(5)	0.1894(2)	0.084(4)
C(3)	0.6180(5)	0.5223(6)	0.1765(2)	0.088(4)
C(4)	0.6112(4)	0.5856(5)	0.1417(2)	0.090(4)
C(5)	0.5131(5)	0.5530(5)	0.1199(2)	0.062(3)
C(6)	0.4218(4)	0.4572(5)	0.13278(13)	0.059(3)
C(7)	0.7117(7)	0.6907(8)	0.1281(4)	0.131(6)
C(8)	0.3295(7)	0.2899(7)	0.1816(3)	0.079(3)
C(9)	0.3349(14)	0.1911(10)	0.1672(6)	0.135(6)
C(10)	0.3097(16)	0.2863(14)	0.2333(4)	0.141(7)
C(11)	0.5029(8)	0.6178(7)	0.0821(2)	0.067(3)
C(12)	0.5492(5)	0.6371(4)	−0.0269(2)	0.087(4)
C(13)	0.5484(6)	0.6815(5)	−0.0694(2)	0.118(6)
C(14)	0.4605(7)	0.6924(5)	−0.0820(2)	0.114(5)
C(15)	0.3735(6)	0.6590(5)	−0.0522(2)	0.092(4)
C(16)	0.3743(5)	0.6146(4)	−0.0097(2)	0.065(3)
C(17)	0.4622(5)	0.6037(3)	0.00293(15)	0.064(3)
C(18)	0.2781(9)	0.6712(8)	−0.0665(4)	0.134(6)
C(19)	0.6453(7)	0.6255(7)	−0.0132(3)	0.104(5)
C(20)	0.6552(13)	0.5416(11)	−0.0406(6)	0.134(6)
C(21)	0.7517(11)	0.7311(10)	−0.0125(10)	0.198(11)
C(22)	0.2830(7)	0.5786(5)	0.0231(3)	0.060(3)
C(23)	0.0653(5)	0.3655(4)	0.1336(2)	0.072(3)
C(24)	0.1562(4)	0.4173(3)	0.1057(2)	0.055(3)
C(25)	0.1446(4)	0.4248(3)	0.0585(2)	0.052(2)
C(26)	0.0420(5)	0.3805(4)	0.0393(2)	0.074(3)
C(27)	−0.0489(4)	0.3287(5)	0.0673(2)	0.093(4)
C(28)	−0.0372(4)	0.3212(5)	0.1144(2)	0.095(5)
C(29)	0.0775(8)	0.3573(8)	0.1849(3)	0.104(5)
C(30)	0.0288(9)	0.3893(8)	−0.0125(3)	0.116(5)
C(31)	−0.029(3)	0.453(2)	−0.0200(7)	0.245(15)
C(32)	−0.0237(18)	0.2863(13)	−0.0399(7)	0.196(10)
C(33)	0.2669(6)	0.4659(6)	0.1259(3)	0.055(3)
C(34*)	0.064(5)	0.046(4)	−0.117(3)	0.30(2)
C(35*)	0.020(5)	0.008(4)	−0.150(3)	0.30(2)
C(36*)	0.099(4)	0.045(3)	−0.074(2)	0.280(17)
C(37*)	0.013(4)	0.011(4)	−0.050(2)	0.271(17)
C(38*)	0.051(4)	0.002(4)	−0.182(3)	0.28(2)
C(39*)	−0.038(5)	0.009(4)	−0.095(3)	0.36(3)

[a] U_{eq} is defined as one-third of the trace of the orthogonalized U_{ij} tensor. The carbon atoms (marked with asterisks) representing guest electron density do not correspond to real atoms in the crystal structure, as discussed in the text.

For structure determination of $C_{10}I_2$/TOT using the measured "h" diffraction data, the average basic host structure determined for C_8I_2/TOT was used as the starting model, and the refinement strategy described above for

TABLE 3
Atomic Coordinates and Equivalent Isotropic Displacement Parameters (U_{eq}) for the Average Basic Host Structure of C_8I_2/TOT at 293 K[a]

Atom	x	y	z	U_{eq} (Å^2)
O(1)	0.3231(4)	0.4224(4)	0.1121(2)	0.0598(14)
O(2)	0.3003(7)	0.5417(7)	0.1521(3)	0.112(3)
O(3)	0.2357(4)	0.4756(4)	0.0310(2)	0.0644(14)
O(4)	0.2523(7)	0.6356(5)	0.0388(3)	0.103(2)
O(5)	0.4617(5)	0.5577(4)	0.0450(2)	0.069(2)
O(6)	0.5404(8)	0.7133(5)	0.0803(3)	0.112(3)
C(1)	0.4289(4)	0.3940(4)	0.16746(13)	0.072(2)
C(2)	0.5270(5)	0.4266(5)	0.18906(15)	0.087(3)
C(3)	0.6181(4)	0.5221(5)	0.1760(2)	0.086(3)
C(4)	0.6110(3)	0.5851(4)	0.1414(2)	0.097(4)
C(5)	0.5129(4)	0.5526(4)	0.11980(14)	0.065(2)
C(6)	0.4218(3)	0.4571(4)	0.13283(12)	0.061(2)
C(7)	0.7116(7)	0.6901(7)	0.1279(4)	0.128(5)
C(8)	0.3290(7)	0.2892(6)	0.1821(2)	0.087(3)
C(9)	0.3330(13)	0.1898(10)	0.1675(5)	0.131(5)
C(10)	0.3082(17)	0.2884(13)	0.2335(3)	0.146(6)
C(11)	0.5026(7)	0.6177(6)	0.0818(2)	0.070(2)
C(12)	0.5499(4)	0.6386(4)	−0.0271(2)	0.093(3)
C(13)	0.5488(5)	0.6833(5)	−0.0693(2)	0.121(5)
C(14)	0.4609(6)	0.6939(5)	−0.08175(15)	0.117(4)
C(15)	0.3739(5)	0.6597(4)	−0.0520(2)	0.090(3)
C(16)	0.3750(4)	0.6150(3)	−0.00973(15)	0.066(2)
C(17)	0.4629(4)	0.6044(3)	0.00271(13)	0.068(2)
C(18)	0.2788(9)	0.6717(7)	−0.0661(3)	0.132(5)
C(19)	0.6458(6)	0.6272(6)	−0.0132(3)	0.121(5)
C(20)	0.6560(13)	0.5434(11)	−0.0404(5)	0.137(5)
C(21)	0.7541(11)	0.7305(10)	−0.0115(9)	0.174(8)
C(22)	0.2815(6)	0.5783(5)	0.0225(2)	0.064(2)
C(23)	0.0653(4)	0.3647(4)	0.13332(14)	0.080(3)
C(24)	0.1559(3)	0.4168(3)	0.10543(15)	0.059(2)
C(25)	0.1442(3)	0.4246(3)	0.05843(14)	0.057(2)
C(26)	0.0417(4)	0.3803(4)	0.03932(15)	0.084(3)
C(27)	−0.0489(3)	0.3282(4)	0.0672(2)	0.096(3)
C(28)	−0.0371(3)	0.3204(4)	0.1142(2)	0.114(5)
C(29)	0.0773(8)	0.3559(8)	0.1846(3)	0.119(5)
C(30)	0.0271(8)	0.3893(7)	−0.0124(3)	0.124(5)
C(31)	−0.024(3)	0.460(3)	−0.0188(6)	0.261(18)
C(32)	−0.022(2)	0.2841(14)	−0.0381(8)	0.221(11)
C(33)	0.2665(5)	0.4653(5)	0.1264(3)	0.062(2)
C(34*)	0.0147(18)	0.024(3)	0.102(2)	0.23(3)
C(35*)	−0.050(3)	−0.0422(17)	0.0696(11)	0.170(10)
C(36*)	0.016(3)	0.036(3)	0.024(2)	0.25(3)
C(37*)	−0.003(2)	0.031(2)	0.150(3)	0.28(3)
C(38*)	−0.017(3)	0.043(3)	0.055(2)	0.209(16)
C(39*)	0.051(2)	0.087(3)	0.0897(16)	0.201(13)

[a] The carbon atoms (marked with asterisks) representing guest electron density do not correspond to real atoms in the crystal structure, as discussed in the text.

C_8I_2/TOT was followed. The final refinement parameters are given in Table 1 and the final refined coordinates are reported in Table 4.

The average basic host structures of $C_{10}Br_2$/TOT, C_8I_2/TOT (Fig. 7), and $C_{10}I_2$/TOT are essentially the same, with the positions of corresponding atoms in these structures differing by less than 3σ in all fractional coordinates. These basic host structures represent the standard structure of the type T-II inclusion compounds of TOT.

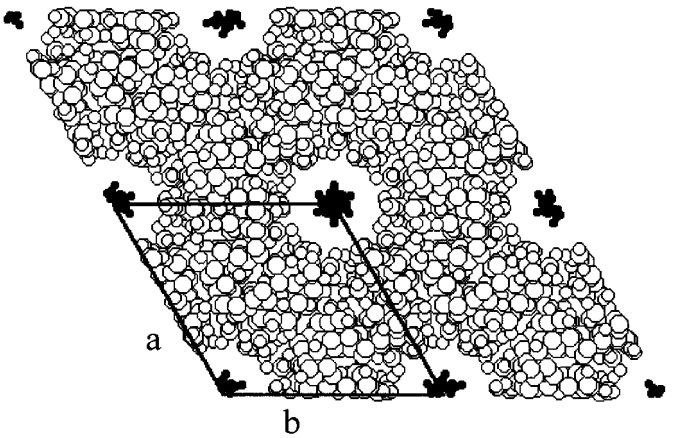

FIG. 7. View along the tunnel axis (c axis) of the average basic host structure in the C_8I_2/TOT inclusion compound at 293 K.

5. CONCLUDING REMARKS

As discussed above, there are no significant differences between the average basic host structures in the $C_{10}Br_2$/TOT, C_8I_2/TOT, and $C_{10}I_2$/TOT inclusion compounds at 293 K, and in all cases there is an incommensurate relationship between the periodicities of the host and guest substructures along the tunnel direction. The periodic repeat distance of the guest molecules along the tunnel is comparable to the length of the guest molecule in the type of linear conformation required to fit within the TOT host tunnel. The fact that the basic host structure is essentially independent of the type of guest molecule is not unexpected given the incommensurate nature of these inclusion compounds. For $C_{10}Br_2$/TOT and $C_{10}I_2$/TOT, additional low-intensity reflections provide evidence for a weak superstructure of the basic host structure. A full characterization of this superstructure will require more appropriate (synchrotron-based) methods for measurement of the weak superstructure reflections. For C_8I_2/TOT, a phase transition occurs at about 136 K. Many solid organic inclusion compounds are known to undergo low-temperature phase transitions that are associated with changes in the symmetry of the host structure and changes in the dynamic properties of the guest molecules. Clearly, further investigations are required to establish the structural and dynamic implications of the phase transition in C_8I_2/TOT. In view of problems due to crystal twinning, future studies of the structural properties of the low-temperature phase will focus on the application of powder diffraction techniques.

TABLE 4
Atomic Coordinates and Equivalent Isotropic Displacement Parameters (U_{eq}) for the Average Basic Host Structure of $C_{10}I_2$/TOT at 293 K[a]

Atom	x	y	z	U_{eq} (Å^2)
O(1)	0.3225(6)	0.4200(6)	0.1119(3)	0.057(2)
O(2)	0.2991(9)	0.5390(9)	0.1519(4)	0.108(4)
O(3)	0.2359(6)	0.4766(6)	0.0311(3)	0.064(2)
O(4)	0.2497(9)	0.6332(8)	0.0389(4)	0.097(4)
O(5)	0.4607(7)	0.5573(5)	0.0459(2)	0.067(3)
O(6)	0.5413(10)	0.7130(8)	0.0810(3)	0.102(4)
C(1)	0.4272(5)	0.3916(5)	0.1677(2)	0.068(4)
C(2)	0.5252(6)	0.4245(6)	0.1897(2)	0.079(4)
C(3)	0.6164(5)	0.5207(6)	0.1770(3)	0.060(3)
C(4)	0.6097(5)	0.5840(5)	0.1424(3)	0.079(5)
C(5)	0.5118(6)	0.5510(5)	0.1204(2)	0.056(3)
C(6)	0.4205(5)	0.4549(6)	0.1330(2)	0.057(3)
C(7)	0.7095(9)	0.6889(8)	0.1289(4)	0.129(8)
C(8)	0.3277(9)	0.2867(8)	0.1817(3)	0.090(5)
C(9)	0.3354(15)	0.1894(12)	0.1677(6)	0.121(7)
C(10)	0.3084(16)	0.2847(14)	0.2330(4)	0.124(8)
C(11)	0.5018(10)	0.6168(8)	0.0827(3)	0.080(5)
C(12)	0.5505(6)	0.6358(5)	−0.0265(2)	0.075(5)
C(13)	0.5501(7)	0.6801(6)	−0.0690(2)	0.122(8)
C(14)	0.4625(8)	0.6912(6)	−0.0818(2)	0.123(8)
C(15)	0.3752(7)	0.6581(5)	−0.0522(2)	0.091(5)
C(16)	0.3755(6)	0.6138(4)	−0.0098(2)	0.057(4)
C(17)	0.4632(6)	0.6027(4)	0.0031(2)	0.081(5)
C(18)	0.2800(10)	0.6703(9)	−0.0664(4)	0.121(7)
C(19)	0.6470(8)	0.6240(8)	−0.0125(4)	0.104(6)
C(20)	0.6567(15)	0.5414(12)	−0.0411(6)	0.117(7)
C(21)	0.7536(12)	0.7307(12)	−0.0108(9)	0.156(10)
C(22)	0.2823(8)	0.5786(6)	0.0221(4)	0.063(4)
C(23)	0.0662(6)	0.3634(5)	0.1335(2)	0.074(5)
C(24)	0.1564(5)	0.4159(4)	0.1052(2)	0.049(3)
C(25)	0.1435(5)	0.4239(4)	0.0584(2)	0.050(3)
C(26)	0.0404(6)	0.3793(6)	0.0397(2)	0.085(5)
C(27)	−0.0498(5)	0.3268(6)	0.0679(3)	0.105(6)
C(28)	−0.0369(5)	0.3188(6)	0.1148(3)	0.094(5)
C(29)	0.0795(10)	0.3544(9)	0.1848(3)	0.097(6)
C(30)	0.0267(11)	0.3887(10)	−0.0116(3)	0.129(8)
C(31)	−0.028(3)	0.454(3)	−0.0197(7)	0.217(16)
C(32)	−0.020(2)	0.2878(16)	−0.0404(8)	0.177(11)
C(33)	0.2666(8)	0.4637(8)	0.1256(4)	0.060(4)
C(34*)	0.0482(18)	0.0171(18)	−0.150(3)	0.54(4)
C(35*)	0.033(2)	0.0195(19)	−0.0885(12)	0.125(12)
C(36*)	0.019(5)	0.026(3)	−0.031(3)	0.41(6)
C(37*)	−0.0253(19)	0.0012(19)	−0.078(2)	0.32(4)
C(38*)	0.067(2)	0.049(2)	−0.115(2)	0.31(3)
C(39*)	0.0846(17)	0.079(2)	0.010(3)	0.88(7)
C(40*)	0.0067(15)	0.0457(17)	−0.1119(13)	0.19(2)

[a] The carbon atoms (marked with asterisks) representing guest electron density do not correspond to real atoms in the crystal structure, as discussed in the text.

While there is well-defined ordering of guest molecules along the tunnel direction (allowing an average periodicity c_g to be defined), there is only a limited extent of three-dimensional (intertunnel) ordering of the guest molecules. However, the diffraction studies reported here (at least at 293 K) provide insufficient information from which to establish the nature of the weak intertunnel ordering. In contrast, for urea inclusion compounds containing the same α,ω-dihalogenoalkane guest molecules, well-defined modes of intertunnel ordering of the guest molecules have been determined (14, 20). The substantially weaker intertunnel ordering of the guest molecules in the TOT inclusion compounds is probably a consequence of the larger distance between neighboring tunnels [14.3 Å (TOT) compared with 8.2 Å (urea)].

Although $C_{10}Br_2$/TOT, C_8I_2/TOT, and $C_{10}I_2$/TOT all have essentially the same basic host structure and an incommensurate relationship between their host and guest substructures, the diffuse scattering in the "g" diffraction pattern differs in subtle ways between these inclusion compounds. However, although a qualitative assessment of the extent and nature of the ordering of the guest molecules may be derived from the types of diffraction photographs reported here, it is important to recall that each diffuse layer line within the "g" diffraction pattern in the oscillation photograph represents two-dimensional diffraction data projected onto a one-dimensional line. To unravel the structural information contained in the two-dimensional sheets of diffuse scattering in the "g" diffraction pattern (and, in particular, to establish the intensity distributions within these sheets), a comprehensive exploration of the "g" diffraction patterns as a function of position in reciprocal space is required. In particular, a complete quantitative scanning of selected two-dimensional regions of reciprocal space is required, ideally with the use of synchrotron radiation and importantly as a function of temperature. Station 16.3 at the Synchrotron Radiation Source (Daresbury Laboratory) provides excellent opportunities for such experiments.

ACKNOWLEDGMENTS

We are grateful to EPSRC for general support (to K.D.M.H.) and the University of Birmingham for the award of a Ph.D. studentship (to H.S.G.).

REFERENCES

1. W. D. Ollis and I. O. Sutherland, *Chem. Commun.*, 402 (1966).
2. S. Brunie and G. Tsoucaris, *Cryst. Struct. Commun.* **3,** 481 (1974).
3. R. Gerdil, *in* "Topics in Current Chemistry" (E. Weber, Ed.), Vol. 140, p. 71. Springer-Verlag, Berlin, 1987.
4. R. Gerdil, *in* "Comprehensive Supramolecular Chemistry" (D. D. MacNicol, F. Toda, and R. Bishop, Eds.), Vol. 6, p. 239. Pergamon, Oxford, 1996.
5. D. Lawton and H. M. Powell, *J. Chem. Soc.*, 2339 (1958).
6. R. Arad-Yellin, B. S. Green, M. Knossow, and G. Tsoucaris, *J. Am. Chem. Soc.* **105,** 4561 (1983).
7. R. Arad-Yellin, B. S. Green, M. Knossow, and G. Tsoucaris, *in* "Inclusion Compounds" (J. L. Atwood, J. E. D. Davies, and D. D. MacNicol, Eds.), Vol. 3, p. 263. Academic Press, New York, 1984.

8. M. D. Hollingsworth and K. D. M. Harris, *in* "Comprehensive Supramolecular Chemistry" (D. D. MacNicol, F. Toda, and R. Bishop, Eds.), Vol. 6, p. 177. Pergamon, Oxford, 1996.
9. K. D. M. Harris and J. M. Thomas, *J. Chem. Soc. Faraday Trans.* **86,** 2985 (1990).
10. H. Serrano-González and K. D. M. Harris, *J. Mol. Struct*., in press.
11. A. J. O. Rennie and K. D. M. Harris, *Proc. R. Soc. A* **430,** 615 (1990).
12. S. van Smaalen, *Crystallogr. Rev*. **4,** 79 (1995).
13. K. D. M. Harris and M. D. Hollingsworth, *Proc. R. Soc. A* **431,** 245 (1990).
14. K. D. M. Harris, S. P. Smart, and M. D. Hollingsworth, *J. Chem. Soc. Faraday Trans*. **87,** 3423 (1991).
15. I. J. Shannon, N. M. Stainton, and K. D. M. Harris, *J. Mater. Chem.* **3,** 1085 (1993).
16. J. M. Gnaim, B. S. Green, R. Arad-Yellin, and P. M. Keehn, *J. Org. Chem.* **56,** 4525 (1991).
17. G. M. Sheldrick, "SHELXL-93, Program for Refinement of Crystal Structures," University of Göttingen, 1993.
18. G. M. Sheldrick, "SHELXL-97, Program for Refinement of Crystal Structures," University of Göttingen, 1997.
19. F. H. Allen, O. Kennard, D. G. Watson, L. Brammer, A. G. Orpen, and R. Taylor, *J. Chem. Soc. Perkin Trans. 2*, S1 (1987).
20. C. L. Bauer, B. M. Kariuki, and K. D. M. Harris, manuscript in preparation.